Scientific Reports

https://doi.org/10.1038/s41598-026-39101-6

Article in Press

Identification of key hub genes in spinal cord ischemia-reperfusion injury via integrated bioinformatics analysis and in vivo validation

Received: 21 June 2025

Accepted: 3 February 2026

Published online: 10 February 2026

Cite this article as: Gao M., Liu H., Sun C. *et al.* Identification of key hub genes in spinal cord ischemia-reperfusion injury via integrated bioinformatics analysis and in vivo validation. *Sci Rep* (2026). https://doi.org/10.1038/s41598-026-39101-6

Mingjie Gao, Haitong Liu, Caixia Sun, Jishan Yuan, Lei Wang & Jinzhong Ma

Identification of Key Hub Genes in Spinal Cord Ischemia-Reperfusion Injury via Integrated Bioinformatics Analysis and In Vivo Validation

Mingjie Gao [1, 2], Haitong Liu [3*], Caixia Sun [3], Jishan Yuan [2], Lei Wang [2], Jinzhong Ma [1, 4*]

1. Department of Orthopedics, Shanghai General Hospital of Nanjing Medical University, Shanghai, 201600, China.
2. Department of Orthopedics, The Affiliated People's Hospital of Jiangsu University, Zhenjiang, Jiangsu, 212002, China.
3. Department of Anesthesiology, The Affiliated People's Hospital of Jiangsu University, Zhenjiang, Jiangsu, 212002, China.
4. Department of Orthopedics, Shanghai General Hospital, Shanghai Jiao Tong University School of Medicine, Shanghai, 201600, China.
*Corresponding. dolinet@163.com, majinzhong1963@sina.com

ABSTRACT

Spinal cord ischemia-reperfusion injury (SCII) often causes neurological damage and devastating sensory and motor dysfunction. Identifying key genes and signaling pathways in SCII progression may provide novel therapeutic targets. Two gene expression datasets (GSE138966 and GSE167274) were obtained from the Gene Expression Omnibus database. Differentially expressed genes were identified using R software, followed by Gene Ontology (GO) and Kyoto Encyclopedia of Genes and Genomes (KEGG) enrichment analyses. Hub genes were screened via Venn analysis, and a protein-protein interaction (PPI) network was constructed using Cytoscape software. Key hub genes were validated by qRT-PCR in a rat SCII model. A total of 99 hub genes were identified, including 60 up-regulated and 39 down-regulated genes. KEGG analysis revealed significant enrichment in MAPK, cAMP, and Rap1 signaling pathways. PPI network analysis highlighted *Ccl2, Mmp9, Itgb1, Timp1, Myd88, and Lgals3* as central nodes. qRT-PCR validation showed persistent up-regulation of *Tnc, Thbs2,* and *S100a10* at 1h, 24h, and 48h post-SCII; early up-regulation of *Msn, Lcp1, Lcn2,* and *Akap12* at 1h; and delayed up-regulation of *Itga5* at 48h ($P < 0.05$). This study identifies novel, key SCII-related genes that have been largely overlooked and, for the first time, defines their time-dependent expression patterns via in vivo experimental validation. Our findings provide crucial mechanistic insights and nominate promising therapeutic targets for SCII.

Introduction

Spinal cord ischemia-reperfusion injury (SCII), a severe complication

associated with aortic surgery or various spinal pathologies, including trauma, degeneration, and tumors, leads to devastating sensory and motor dysfunction [1]. The fundamental mechanism of SCII lies in calcium overload and metabolite accumulation, which are triggered by energy metabolism disorders during the ischemic phase. Subsequently, during the reperfusion stage, tissue damage is further exacerbated through the activation of oxidative stress bursts, inflammatory cascades, as well as apoptosis and necrosis pathways [2,3]. Although current therapeutic approaches, such as early surgical decompression, cerebrospinal fluid drainage, vascular interventions, steroid administration, and antioxidant use, can alleviate the damage to a certain degree, they are ineffective in halting the progression of paraplegia [4-6]. Therefore, a comprehensive and systematic investigation is urgently needed to identify effective therapeutic targets and develop more efficacious treatment strategies.

Bioinformatics, an interdisciplinary field, serves as a powerful tool for elucidating disease mechanisms by decoding molecular networks [7]. By delving deeper into these molecular networks and the genes that constitute them, we can gain crucial insights into the pathogenesis of SCII. With the recent rapid advancements in microarray and high-throughput sequencing technologies, it has become possible to rapidly detect differentially expressed genes (DEGs) and conduct multi-timepoint analyses of SCII progression [8]. For instance, Zhou et al. [9] utilized high-throughput RNA sequencing to identify differentially expressed long non-coding RNAs (lncRNAs) and messenger RNAs (mRNAs) in the spinal cords of rats after SCII. This study revealed genome-wide expression patterns of lncRNAs and mRNAs in the spinal cords post-SCII, suggesting that these RNAs may play pivotal roles in the pathophysiological processes following SCII. Furthermore, by utilizing transcriptomic analysis of photothrombotically induced ischemic lesions in the cerebral cortex and spinal cord, Pavic et al.[10] investigated inflammatory responses and repair activities in the ischemic brain and spinal cord between day 1 and day 7 post-ischemia. Based on these research results, it is evident that potential key genes with significant expression in SCII and involvement in pathological and physiological changes should be identified. However, to date, such genes remain largely unknown.

In this study, we applied bioinformatic analysis methods to screen for DEGs between SCII samples and control samples. Through the characterization of dysregulated hub genes and key pathways, we aimed to enhance the systems-level understanding of SCII mechanisms. Moreover, by integrating bioinformatics predictions with quantitative polymerase chain reaction (qPCR) validation in a rat SCII model, we sought to strengthen the reliability of our research results.

Results

Identification of DEGs in GSE138966 and GSE167274

Bioinformatics analysis was conducted following the workflow outlined in **Figure 1S**. DEGs were identified separately in GSE138966 and GSE167274 datasets. Specifically, we analyzed DEGs between control and SCII groups at 48 hours rat post-SCII in GSE138966, and at 1-day, 3-day, and 7-day C57BL/6J mice post-SCII in GSE167274. In GSE138966，a total of 278 DEGs were identified (|logFC| > 1, P.adj < 0.05), including 256 up-regulated and 22 down-regulated genes (**Supplemental Document 1**). In GSE167274，time-course analysis revealed: 2438 DEGs (1176 up-regulated, 1262 down-regulated) were identified at 1-day post-SCII; 2933 DEGs (1687 up-regulated, 1246 down-regulated) were identified at 3-day post-SCII; and 3810 DEGs (2100 up-regulated, 1710 down-regulated) were identified at 7-day post-SCII (|logFC| > 1, P.adj < 0.05)(**Supplemental Document 2**). Heatmaps (**Figure 1**) and volcano plots (**Figure 2**) visualized DEG expression profiles between control and SCII groups. For GSE167274, time-series analysis based on transcriptional dynamics stratified SCII samples into 16 clusters (**Figure 2S and Supplemental Document 3**). Cluster membership ranged from 622 (Cluster 12) to 1,610 genes (Cluster 6), with red/purple lines indicating high membership and yellow/green lines indicating low membership.

Functional Enrichment Analysis of DEGs via GO and KEGG Pathways

GO and KEGG enrichment analyses were performed to annotate DEG functions. The top 10 GO terms for GSE138966 and GSE167274 was displayed in **Figure 3**, respectively. KEGG pathway analysis identified top 20 enriched pathways (**Figure 4**). Based on these data, the five core pathways and their respective associated hub genes are presented in **Figure 3S**. In particular, the MAPK signaling pathway in GSE138966 primarily involves the genes *Epha2, Dusp2, Flt1, Angpt2, Il1a, Rps6ka3, Artn, Flnc, Ereg, Dusp5, Gadd45g, Nfkb2, Cd14, Myd88, Gadd45b, Bcl2a1, Map2k3, Nfkb1,* and *Map3k8*. In GSE167274, this pathway mainly includes the genes *Nlk, Cacng3, Fgfr1, Map3k10, Ret, Rasgrp1, Myc, Nfkb2, Akt3, Nr4a1, Cd14, Irak4, Rela, Myd88,* and *Gadd45g* (**Figure 3S**). Besides, the relationships among key pathways were also revealed respectively (**Figure 4S**). Then Venn analysis was used for overlapped KEGG pathways at 1-day, 3-day and 7-day after C57BL/6J mice SCII in GSE167274 (**Figure 5S**). Dynamic pathway enrichment was performed based on Venn analysis of three time points after SCII in GSE167274, with MAPK, cAMP, and Rap1 signaling pathways emerging as central to SCII pathogenesis (**Figure 5**).

PPI Network of Hub Genes

To explore the common genes with persistently abnormal expression during the SCII process, we conducted an integrated analysis of DEGs from the two datasets. For homologous mapping, we retrieved homologous gene datasets between rats and mice from the Ensembl database (https://mart.ensembl.org/index.html; Ensembl Release 115, August 2025)(see **Supplemental Document 4**). Subsequently, we integrated the DEG results

of the two datasets based on homologous mapping (**Supplemental Documents 5 & 6**). Since the SCII-related datasets in GSE167274 are divided into three time points (1-day, 3-day, and 7-day post-SCII), we performed Venn analysis based on three sets of DEG results integrated via homologous mapping (**Supplemental Document 7**). A total of 64 hub genes (|logFC| > 1, P.adj < 0.05) and 21 hub genes (|logFC| > 2, P.adj < 0.05) were obtained (**Figure 6S**). Focusing on DEGs with |logFC| > 2, key hubs included *Tm4sf1*, *Tnc*, *Thbs1*, *Bcl2a1b*, *Bcl2a1a*, *Bcl2a1d*, *S100a10*, *Plin2*, *Timp1*, *Lcp1*, *Itga5*, *Csf2rb2*, *Tagln2*, *Fcgr2b*, *Fcgr3*, *Thbs2*, *Msn*, *Pdpn*, *Lgals3*, *Lcn2* and *Akap12*, all of which were up-regulated. Based on these results, PPI networks for rats and mice were constructed separately using STRING and visualized in Cytoscape (**Figure 6**).

According to the Cytoscape analysis results, the network of 64 DEGs (|logFC| > 1, P.adj < 0.05) in the rat organism ultimately contained 40 nodes, 274 edges, and the average number of neighbors was 6.85. Notably, in rat tissue, *Ccl2* was connected to 44 DEGs, *Mmp9* to 38, *Itgb1* to 32, *Lgals3* to 28, *Myd88* to 28, *Thbs1* to 26, and *Timp1* to 22. Meanwhile, in the network of 64 DEGs (|logFC| > 1, P.adj < 0.05) in the mouse organism, there were 44 nodes, 364 edges, and the average number of neighbors was 8.273. Similarly, in mouse tissue, *Ccl2* was connected to 48 DEGs, *Mmp9* to 46, *Itgb1* to 40, *Timp1* to 34, *Fcgr3* to 32, *Myd88* to 30, and *Lgals3* to 30.

In Vivo Validation of Hub Genes

SCII rat models were established to validate hub gene expression. The hind limb motor function between sham and SCII group was recorded using BBB scoring system (**Figure 7S**). It showed significantly lower motor function in SCII group compared to Sham group at all time points following spinal cord ischemia (P < 0.05). According to the biological function and the result of bioinformatic analysis, eight more promising and previously understudied hub genes (*Tnc, Thbs2, S100a10, Msn, Lcp1, Lcn2, Akap12,* and *Itga5*) in SCII were selected to validate the expression levels in vivo (**Table 1**). As shown in **Figure 7**, the expression of *Tnc*, *Thbs2*, and *S100a10* was markedly elevated at 1h, 24h, and 48h post-ischemia, demonstrating a sustained activation pattern throughout the early and sub-acute phases of SCII. In contrast, a distinct cluster of genes, including *Msn*, *Lcp1*, *Lcn2*, and *Akap12*, exhibited a transient early response, with significant up-regulation observed only at the 1h time point. The expression of *Itga5* was significantly increased specifically at 48h, suggesting a role in the delayed pathological processes. These results robustly align with our bioinformatics predictions, experimentally confirming the involvement of these hub genes in SCII pathogenesis.

Gene	Protein	Function	Ref.

Lcn2	Neutrophil gelatinase-associated lipocalin	Involve in multiple processes such as apoptosis, innate immunity and renal development.	20
Itga5	Integrin alpha-5	A receptor for fibronectin and fibrinogen. It recognizes the sequence R-G-D in its ligands.	21
Akap12	A-kinase anchor protein 12	Anchoring protein that mediates the subcellular compartmentation of protein kinase A (PKA) and protein kinase C (PKC).	22
Tnc	Tenascin	Extracellular matrix protein implicated in guidance of migrating neurons as well as axons during development, synaptic plasticity as well as neuronal regeneration.	23
Lcp1	Plastin-2	Plays a role in the activation of T-cells in response to costimulation through TCR/CD3 and CD2 or CD28. Modulates the cell surface expression of IL2RA/CD25 and CD69.	24
S100a10	Protein S100-A10	As a regulator of protein phosphorylation in that the ANXA2 monomer is the preferred target (in vitro) of tyrosine-specific kinase.	25
Msn	Moesin	Ezrin-radixin-moesin (ERM) family protein that connects the actin cytoskeleton to the plasma membrane and thereby regulates the structure and function of specific domains of the cell cortex. The role of moesin is particularly important in immunity acting on both T and B-cells homeostasis and self-tolerance, regulating lymphocyte egress from lymphoid organs.	26, 27
Thbs2	Thrombospondin-2	Adhesive glycoprotein that mediates cell-to-cell and cell-to-matrix interactions. Ligand for CD36 mediating antiangiogenic properties.	28

Table 1. Details of selected hub genes

Discussion

SCII represents a critical form of secondary spinal cord injury, primarily driven by oxidative stress imbalance and inflammation respond within the spinal cord microenvironment [29]. Identifying novel biomarkers for early diagnosis, targeted therapy, and prognosis of SCII holds significant clinical value [30]. Microarray and high-throughput technologies are pivotal tools for investigating gene expression profiles and deciphering the molecular mechanisms underlying complex diseases. In this study, integrated analysis of microarray datasets has enhanced our understanding of SCII pathogenesis and revealed temporally dynamic molecular signatures with prognostic implications. Here, we analyzed DEGs from two independent datasets (GSE138966 and GSE167274) comparing SCII and control samples. Venn

analysis identified key hub genes which were significantly up-regulated in SCII tissues. These genes are implicated in inflammatory signaling, extracellular matrix remodeling, and cell adhesion key processes in SCII pathophysiology.

The constructed PPI network revealed functionally interconnected modules mediating critical biological processes in SCII, including signal transduction, transcriptional regulation, and inflammatory cascades. Cytoscape visualization highlighted *Ccl2* as the most central node (connected to 48 DEGs), followed by *Mmp9* (44 DEGs), *Itgb1* (38 DEGs), *Timp1* (34 DEGs), *Myd88* (30 DEGs), and *Lgals3* (28 DEGs). These findings align with prior studies. The *Ccl2/Ccr2* axis amplifies monocyte-driven tissue damage in inflammatory diseases [31,32]. *Mmp9* inhibition improves spinal cord injury recovery by reducing neuronal apoptosis and preserving blood-spinal cord barrier integrity [33,34]. Notably, *Myd88* acts as a central hub in inflammatory signaling, which can induce signaling from several receptors, located either at the plasma membrane or in endosomes [35,36]. *Lgals3* has been linked to myocardial ischemia-reperfusion injury [37]. Yan et al. [38] reported up-regulation of *S100a10*, *Timp1*, and *Lgals3* in injured neurons and sub-acute spinal cord injury models, which was further validated our findings.

Functional enrichment analysis via GO and KEGG pathways provided mechanistic insights into SCII. KEGG analysis revealed significant enrichment of MAPK, cAMP, and Rap1 signaling pathways across time points in GSE167274. The MAPK pathway modulates post-injury inflammatory responses by modulating cytokine and chemokine expression, while p38-MAPK activation drives secondary SCII apoptosis [39,40]. Activation of the Epac/Rap1 pathway could alleviates brain ischemia-reperfusion injury [41], suggesting conserved mechanisms across central nervous system injury models. Collectively, these pathways represent promising therapeutic targets for mitigating secondary injury in SCII.

Based on hub gene functions and their roles in the central nervous system, eight key genes were selected for expression validation. Tenascin-C (TNC), an extracellular matrix protein, guides neuronal/axonal migration during development and regulates synaptic plasticity and regeneration. It promotes neurite outgrowth in cultured neurons and is up-regulated in inflammatory conditions (e.g., traumatic injury, bacterial infection) [42,43]. Thrombospondin-2 (THBS2), a secreted matrix protein, modulates angiogenesis, tissue remodeling, and inflammation by mediating cell-matrix interactions [44,45]. S100A10 exhibits neuroprotective effects via the cerebral fibrinolytic system, serving as both a stroke damage mitigator and thrombolytic therapy enhancer [46,47]. Moesin (MSN) links the plasma membrane to the actin cytoskeleton and induces autoimmune responses in aging mice [48]. Lymphocyte cytosolic protein 1 (LCP1) influences neuroinflammation and ischemic brain injury, with LCP1 inhibition reducing brain damage [49]. Lipocalin-2 (LCN2) regulates cell death, inflammation, and iron transport, contributing to neuroinflammation and neuronal death in brain injury models [50,51]. A-kinase anchor protein 12

(AKAP12) stabilizes cellular structures and restricts immune cell infiltration in fibrotic scars, promoting central nervous system recovery [52]. Integrin alpha-5 (ITGA5), expressed in immune cells, correlates with immune infiltration [53].

In vivo RT-PCR validation showed that *Tnc*, *Thbs2*, and *S100a10* were significantly up-regulated at 1, 24, and 48 hours post-SCII. *Msn*, *Lcp1*, *Lcn2*, and *Akap12* were up-regulated at 1 hour, while *Itga5* exhibited delayed up-regulation at 48 hours. It may support the prognostic value of these selected hub genes and pathways, positioning them as promising biomarkers and therapeutic targets for SCII.

This study has several limitations. First, it relies on secondary analysis of existing microarray datasets (GSE138966 and GSE167274) without independent in vivo high-throughput sequencing, which may introduce batch effects or dataset-specific biases. Second, while we validated eight hub genes, the functional characterization of their downstream signaling pathways remains unaddressed. Future studies should integrate multi-omics approaches (e.g., proteomics and metabolomics) to explore SCII mechanisms comprehensively and validate candidate biomarkers in clinical cohorts.

In summary, this bioinformatics-driven study characterizes gene expression profiles and molecular pathways in SCII, identifying dysregulated inflammatory signaling, cell adhesion networks, and tissue remodeling pathways as central to pathogenesis. We further identified and validated eight up-regulated hub genes, many of which have been relatively neglected in SCII research. Among these, *Tnc*, *Thbs2*, and *S100a10* demonstrated persistent up-regulation across the injury timeline, marking them as central and sustained contributors to pathogenesis. These findings provide mechanistic insights and nominate potential therapeutic targets and biomarkers for SCII, warranting further translational investigation.

Methods

Microarray Data Source

The datasets GSE138966 [9] and GSE167274 [10] were downloaded from the Gene Expression Omnibus (GEO) database. GSE138966 represents a high-throughput sequencing-based expression profiling dataset generated using the Illumina HiSeq 4000 platform for Rattus norvegicus. This microarray dataset includes six spinal cord samples: three control samples and three injury samples collected 48 hours after spinal cord ischemia-reperfusion. GSE167274 is an array-based expression profiling dataset utilizing the Affymetrix Clariom S Assay (including Pico Assay) for C57BL/6J mice. The dataset comprises 32 samples in total, covering lesions in both the cerebral cortex and spinal cord across days 1 to 7 post-ischemia. Of particular focus were spinal cord lesion samples, which included three control and three ischemic samples per group at each time point (1-day, 3-day, and 7-day) after

ischemia.

Data processing

Identification of SCII-Related Differentially Expressed Genes

Differential gene expression analysis was performed using the "limma" package in R [11] on control and ischemic spinal cord samples from GSE138966 and GSE167274, respectively, to characterize gene expression alterations associated with SCII. DEGs were identified using thresholds of absolute $\log_2$ fold change (|logFC|) > 1 and adjusted p-value (P.adj) < 0.05. Volcano plots and heat maps were generated to visualize DEG profiles for GSE138966 and GSE167274.

To characterize dynamic gene expression patterns at different time points post-SCII in GSE167274, a soft clustering approach was applied using the Mfuzz package in R. This method assigned genes to multiple clusters based on their expression similarity, with normalization performed using a min.std value of 0.1. Genes with high membership values in specific clusters (calculated by the acore function) were considered functionally similar.

GO and KEGG Pathway Enrichment Analysis

To explore the biological functions and signaling pathways involved in differential hub genes, the R package 'clusterProfiler'[12] was used for gene ontology (GO) and Kyoto Encyclopedia of Genes and Genomes (KEGG) enrichment analysis. GO analysis includes three categories: biological processes (BP), molecular functions (MF), and cellular components (CC). The KEGG database is employed to identify enriched biological pathways [13]. Enrichment analyses for GO terms and KEGG pathways were conducted using the clusterProfiler package in R[14], with statistical significance defined as P.adj< 0.05. GO terms were categorized into BP, CC, and MF functional groups.

Protein-Protein Interaction (PPI) Network Construction

PPI networks are constructed to visualize and analyze functional interactions among proteins, which are involved numerous activities of life processes, such as biological signaling, control of gene expression, energy and material metabolism, and cell cycle regulation [15]. DEGs identified via Venn diagram analysis were uploaded to the STRING database (version: 12.0; https://string-db.org/) [16], to generate PPI networks depicting known and predicted interactions. Network visualization was performed using Cytoscape (v3.10.2) (https://cytoscape.org/download.html)[17], where node size and edge thickness represented interaction confidence: red nodes with thick dark blue edges indicated high-degree nodes, while yellow nodes with thin light blue edges denoted low-degree nodes. Hub genes with the highest connectivity were positioned centrally in the network.

Animal Model Establishment and Hub Gene Validation

This study was performed in accordance with relevant guidelines and regulations. All methods were reported in accordance with ARRIVE guidelines, and all animal experiments were approved by the Experimental Animal Ethics Committee of Jiangsu University (No. 11974, China). Healthy male Sprague-Dawley (SD) rats (280–310g) were obtained from the Animal Experimental Center of Jiangsu University and randomized into Sham (n=6) and SCII (n=6) groups. SCII models were established as previously described [18]: rats were anesthetized with isoflurane (#R510-22-10, RWD Life Science, Shenzhen, China), and a midline abdominal incision was made to expose the aorta. Heparin was administered intravenously 5 min before aortic clamping to prevent thrombosis. The aorta was clamped below the left renal artery using bulldog clamps for 1 hour, followed by reperfusion upon clamp removal. At the end of surgery, gentamicin (40,000 U) was administered intraperitoneally to prevent infection, and incisions were closed with silk sutures. In the sham group, the surgical procedure was performed in the same sequence but without aortic occlusion. Rats were housed in sterile cages with ad libitum access to food and water.

Neurobehavioral Evaluation

Hindlimb motor function was assessed using the Basso, Beattie, and Bresnahan (BBB) scale [19] at 1h, 6h, 24h, and 48h post-ischemia. The BBB scale evaluates hindlimb movement, trunk stability, gait coordination, claw placement, and tail position (0 = complete paralysis, 21 = normal function). Two independent observers blinded to group assignments evaluated scores, and mean values were calculated.

Real-time Quantitative PCR (qRT-PCR)

Rats were euthanized under isoflurane anesthesia, and L4-L6 spinal cord segments were harvested and stored in TRIzol (#15596-018, Invitrogen). Total RNA was extracted using a commercial kit (Vazyme Biotech, Nanjing, China), and RNA concentration was quantified using a NanoDrop™ One spectrophotometer (Thermo Fisher Scientific, USA). Complementary DNA (cDNA) was synthesized using MiniAmp™ Plus Thermal Cycler and SYBR Green qPCR Mix (Vazyme Biotech, Nanjing, Jiangsu Province, China). Primers for *Tnc, Thbs2, S100a10, Msn, Lcp1, Lcn2, Akap12* and *Itga5* were designed via NCBI and synthesized by Sangon Biotech (Shanghai, China) (**Table 1S**). qRT-PCR was performed on an Applied Biosystems™ 7500 system using SYBR Green Master Mix (Vazyme Biotech), with GAPDH as the internal control. Relative gene expression was calculated using the $2^{-\Delta\Delta Ct}$ method across three independent experiments.

Statistical Analysis

Data analysis was conducted using the R programming language (R Studio, v4.3.0) (https://www.r-project.org/) and GraphPad Prism 9. mRNA expression

levels are presented as mean ± standard deviation (SD) from three biological replicates. The BBB scoring data were analyzed using non-parametric method and compared using the Kruskal–Wallis test followed by the Mann–Whitney U-test. Student's t-tests were used to compare hub gene expression between Sham and SCII groups. All statistical tests were two-sided, and $P < 0.05$ was considered significant.

Acknowledgements

This study was supported by Zhenjiang Science and Technology Plan Project-Social Development (Grant No. SH2023061), the Research Fund of the First People's Hospital of Zhenjiang (Grant No. Y2020012) and the Third Phase of "Jinshan Doctors" - Young Talents in Medical Field of Zhenjiang City.

Author contributions statement

G.M. contributed to the study design, analysis, and interpretation of data and drafted the manuscript. L.H. and M.J. contributed to the study design and interpretation of the data, revised the manuscript and approved the final version. S.C. , W.L. and Y.J. critically revised the manuscript and approved the final manuscript. All authors reviewed the manuscript.

Competing interests

The authors declare no competing interests.

Data availability

The datasets selected in our research can be found and downloaded for free online. GEO Database accession number: GSE138966, GSE167274. All data generated or analysed during this study are included in this published article and its supplementary information files.

References

1. Sueda, T. & Takahashi, S. Spinal cord injury as a complication of thoracic endovascular aneurysm repair. *Surg Today.* **48**, 473-477, DOI:10.1007/s00595-017-1588-5 (2018).
2. Kong, X. & Gao, J. Macrophage polarization: a key event in the secondary phase of acute spinal cord injury. *J Cell Mol Med.* **21**, 941-954, DOI:10.1111/jcmm.13034 (2017).
3. Stenudd, M., Sabelstrom, H. & Frisen, J. Role of endogenous neural stem cells in spinal cord injury and repair. *JAMA Neurol.* **72**, 235-237, DOI:10.1001/jamaneurol.2014.2927 (2015).
4. Henmi, S., Ikeno, Y., Yokawa, K., Gotake, Y., Nakai, H., Yamanaka, K., . . . Okita, Y. Comparison of early patency rate and long-term outcomes of various techniques for reconstruction of segmental arteries during

thoracoabdominal aortic aneurysm repair. *Eur J Cardiothorac Surg.* DOI:10.1093/ejcts/ezz015 (2019).

5. Jin, W., Botchway, B. O. A. & Liu, X. Curcumin Can Activate the Nrf2/HO-1 Signaling Pathway and Scavenge Free Radicals in Spinal Cord Injury Treatment. *Neurorehabil Neural Repair.* **35**, 576-584, DOI:10.1177/15459683211011232 (2021).
6. Liu, W. Z., Ma, Z. J., Li, J. R. & Kang, X. W. Mesenchymal stem cell-derived exosomes: therapeutic opportunities and challenges for spinal cord injury. *Stem Cell Res Ther.* **12**, 102, DOI:10.1186/s13287-021-02153-8 (2021).
7. Orlov, Y. L., Anashkina, A. A., Klimontov, V. V. & Baranova, A. V. Medical Genetics, Genomics and Bioinformatics Aid in Understanding Molecular Mechanisms of Human Diseases. *Int J Mol Sci.* **22**, DOI:10.3390/ijms22189962 (2021).
8. Wang, D., Wang, L., Han, J., Zhang, Z., Fang, B., & Chen, F. Bioinformatics-Based Analysis of the lncRNA-miRNA-mRNA Network and TF Regulatory Network to Explore the Regulation Mechanism in Spinal Cord Ischemia/Reperfusion Injury. *Front Genet.* **12**, 650180, DOI:10.3389/fgene.2021.650180 (2021).
9. Zhou, Z., Han, B., Jin, H., Chen, A. & Zhu, L. Changes in long non-coding RNA transcriptomic profiles after ischemia-reperfusion injury in rat spinal cord. *PeerJ.* **8**, e8293, DOI:10.7717/peerj.8293 (2020).
10. Pavic, G., Petzsch, P., Jansen, R., Raba, K., Rychlik, N., Simiantonakis, I., . . . Gliem, M. Microglia contributes to remyelination in cerebral but not spinal cord ischemia. *Glia.* **69**, 2739-2751, DOI:10.1002/glia.24068 (2021).
11. Ritchie, M. E., Phipson, B., Wu, D., Hu, Y., Law, C. W., Shi, W., & Smyth, G. K. limma powers differential expression analyses for RNA-sequencing and microarray studies. *Nucleic Acids Res.* **43**, e47, DOI:10.1093/nar/gkv007 (2015).
12. Wilkerson, M. D. & Hayes, D. N. ConsensusClusterPlus: a class discovery tool with confidence assessments and item tracking. *Bioinformatics.* **26**, 1572-1573, DOI:10.1093/bioinformatics/btq170 (2010).
13. Kanehisa, M. & Goto, S. KEGG: kyoto encyclopedia of genes and genomes. *Nucleic Acids Res.* **28**, 27-30, DOI:10.1093/nar/28.1.27 (2000).
14. Yu, G., Wang, L. G., Han, Y. & He, Q. Y. clusterProfiler: an R package for comparing biological themes among gene clusters. *OMICS.* **16**, 284-287, DOI:10.1089/omi.2011.0118 (2012).
15. Hu, X., Ni, S., Zhao, K., Qian, J. & Duan, Y. Bioinformatics-Led Discovery of Osteoarthritis Biomarkers and Inflammatory Infiltrates. *Front Immunol.* **13**, 871008, DOI:10.3389/fimmu.2022.871008 (2022).
16. Szklarczyk, D., Gable, A. L., Lyon, D., Junge, A., Wyder, S., Huerta-Cepas, J., . . . Mering, C. V. STRING v11: protein-protein association networks with increased coverage, supporting functional discovery in genome-wide experimental datasets. *Nucleic Acids Res.* **47**, D607-D613, DOI:10.1093/nar/gky1131 (2019).

17. Shannon, P., Markiel, A., Ozier, O., Baliga, N. S., Wang, J. T., Ramage, D., . . . Ideker, T. Cytoscape: a software environment for integrated models of biomolecular interaction networks. *Genome Res.* **13**, 2498-2504, DOI:10.1101/gr.1239303 (2003).
18. Yin, F., Guo, L., Meng, C. Y., Liu, Y. J., Lu, R. F., Li, P., & Zhou, Y. B. Transplantation of mesenchymal stem cells exerts anti-apoptotic effects in adult rats after spinal cord ischemia-reperfusion injury. *Brain Res.* **1561**, 1-10, DOI:10.1016/j.brainres.2014.02.047 (2014).
19. Basso, D. M., Beattie, M. S. & Bresnahan, J. C. Descending systems contributing to locomotor recovery after mild or moderate spinal cord injury in rats: experimental evidence and a review of literature. *Restor Neurol Neurosci.* **20**, 189-218 (2002).
20. Yang, J., Goetz, D., Li, J. Y., Wang, W., Mori, K., Setlik, D., . . . Barasch, J. An iron delivery pathway mediated by a lipocalin. *Mol Cell,* **10**, 1045-1056. doi: 10.1016/s1097-2765(02)00710-4 (2002).
21. Kuramoto, K., Liang, H., Hong, J. H., & He, C. Exercise-activated hepatic autophagy via the FN1-α5β1 integrin pathway drives metabolic benefits of exercise. *Cell Metab,* **35**, 620-632 e625. doi: 10.1016/j.cmet.2023.01.011 (2023).
22. Gelman, I. H. Emerging Roles for SSeCKS/Gravin/AKAP12 in the Control of Cell Proliferation, Cancer Malignancy, and Barriergenesis. *Genes Cancer,* **1**, 1147-1156. doi: 10.1177/1947601910392984 (2010).
23. Morellini, F., & Schachner, M. (2006). Enhanced novelty-induced activity, reduced anxiety, delayed resynchronization to daylight reversal and weaker muscle strength in tenascin-C-deficient mice. *Eur J Neurosci,* **23**, 1255-1268. doi: 10.1111/j.1460-9568.2006.04657.x
24. Wabnitz, G. H., Köcher, T., Lohneis, P., Stober, C., Konstandin, M. H., Funk, B., . . . Samstag, Y. Costimulation induced phosphorylation of L-plastin facilitates surface transport of the T cell activation molecules CD69 and CD25. *Eur J Immunol,* **37**, 649-662. doi: 10.1002/eji.200636320 (2007).
25. Madureira, P. A., O'Connell, P. A., Surette, A. P., Miller, V. A., & Waisman, D. M.. The biochemistry and regulation of S100A10: a multifunctional plasminogen receptor involved in oncogenesis. *J Biomed Biotechnol,* **2012**, 353687. doi: 10.1155/2012/353687 (2012)
26. Huang, L., Wong, T. Y., Lin, R. C., & Furthmayr, H. Replacement of threonine 558, a critical site of phosphorylation of moesin in vivo, with aspartate activates F-actin binding of moesin. Regulation by conformational change. *J Biol Chem,* **274**, 12803-12810. doi: 10.1074/jbc.274.18.12803 (1999).
27. Serrador, J. M., Nieto, M., Alonso-Lebrero, J. L., del Pozo, M. A., Calvo, J., Furthmayr, H., . . . Sánchez-Madrid, F.. CD43 interacts with moesin and ezrin and regulates its redistribution to the uropods of T lymphocytes at the cell-cell contacts. *Blood,* **91**, 4632-4644. (1998)
28. Simantov, R., Febbraio, M., & Silverstein, R. L. The antiangiogenic effect of thrombospondin-2 is mediated by CD36 and modulated by histidine-rich

glycoprotein. *Matrix Biol,* **24**, 27-34. doi: 10.1016/j.matbio.2004.11.005 (2005).

29. Alizadeh, A., Dyck, S. M. & Karimi-Abdolrezaee, S. Traumatic Spinal Cord Injury: An Overview of Pathophysiology, Models and Acute Injury Mechanisms. *Front Neurol.* **10**, 282, DOI:10.3389/fneur.2019.00282 (2019).
30. Hutson, T. H. & Di Giovanni, S. The translational landscape in spinal cord injury: focus on neuroplasticity and regeneration. *Nat Rev Neurol.* **15**, 732-745, DOI:10.1038/s41582-019-0280-3 (2019).
31. Jiang, W., Xu, T., Song, Z., Wang, X., Yuan, S., Li, Q., . . . Hu, W. CCL2 is a key regulator and therapeutic target for periodontitis. *J Clin Periodontol.* **50**, 1644-1657, DOI:10.1111/jcpe.13872 (2023).
32. Du, S., Wu, S., Feng, X., Wang, B., Xia, S., Liang, L., . . . Tao, Y. X. A nerve injury-specific long noncoding RNA promotes neuropathic pain by increasing Ccl2 expression. *J Clin Invest.* **132**, DOI:10.1172/jci153563 (2022).
33. Lee, J. Y., Kim, H. S., Choi, H. Y., Oh, T. H. & Yune, T. Y. Fluoxetine inhibits matrix metalloprotease activation and prevents disruption of blood-spinal cord barrier after spinal cord injury. *Brain.* **135**, 2375-2389, DOI:10.1093/brain/aws171 (2012).
34. Rempe, R. G., Hartz, A. M. S. & Bauer, B. Matrix metalloproteinases in the brain and blood-brain barrier: Versatile breakers and makers. *J Cereb Blood Flow Metab.* **36**, 1481-1507, DOI:10.1177/0271678x16655551 (2016).
35. Wang, Q., Cun, D., Xu, D., Lin, L., Jiao, J., Zhang, L., . . . Hu, M. Myd88 knockdown with RNA interference induces in vitro immune hyporesponsiveness in dendritic cells from rhesus monkeys. *Immunogenetics.* **74**, 303-312, DOI:10.1007/s00251-022-01260-x (2022).
36. Bayer, A. L. & Alcaide, P. MyD88: At the heart of inflammatory signaling and cardiovascular disease. *J Mol Cell Cardiol.* **161**, 75-85, DOI:10.1016/j.yjmcc.2021.08.001 (2021).
37. Rong, J., Pan, H., He, J., Zhang, Y., Hu, Y., Wang, C., . . . Zheng, Z. Long non-coding RNA KCNQ1OT1/microRNA-204-5p/LGALS3 axis regulates myocardial ischemia/reperfusion injury in mice. *Cell Signal.* **66**, 109441, DOI:10.1016/j.cellsig.2019.109441 (2020).
38. Yan, L., Li, Z., Li, C., Chen, J., Zhou, X., Cui, J., . . . Cui, Z. Hspb1 and Lgals3 in spinal neurons are closely associated with autophagy following excitotoxicity based on machine learning algorithms. *PLoS One.* **19**, e0303235, DOI:10.1371/journal.pone.0303235 (2024).
39. Tavares, L. P., Negreiros-Lima, G. L., Lima, K. M., PMR, E. Silva, Pinho, V., Teixeira, M. M., & Sousa, L. P. Blame the signaling: Role of cAMP for the resolution of inflammation. *Pharmacol Res.* **159**, 105030, DOI:10.1016/j.phrs.2020.105030 (2020).
40. Xu, Z., Wang, B. R., Wang, X., Kuang, F., Duan, X. L., Jiao, X. Y., & Ju, G. ERK1/2 and p38 mitogen-activated protein kinase mediate iNOS-induced spinal neuron degeneration after acute traumatic spinal cord injury. *Life Sci.* **79**, 1895-1905, DOI:10.1016/j.lfs.2006.06.023 (2006).

41. Sun, X., Wang, Y., Zhao, Y., Xu, X., Lu, W., Li, Y., . . . Zhou, L. Activation of the Epac/Rap1 signaling pathway alleviates blood-brain barrier disruption and brain damage following cerebral ischemia/reperfusion injury. *Int Immunopharmacol.* **117**, 110014, DOI:10.1016/j.intimp.2023.110014 (2023).
42. Midwood, K. S., Chiquet, M., Tucker, R. P. & Orend, G. Tenascin-C at a glance. *J Cell Sci.* **129**, 4321-4327, DOI:10.1242/jcs.190546 (2016).
43. Midwood, K., Sacre, S., Piccinini, A. M., Inglis, J., Trebaul, A., Chan, E., . . . Foxwell, B. Tenascin-C is an endogenous activator of Toll-like receptor 4 that is essential for maintaining inflammation in arthritic joint disease. *Nat Med.* **15**, 774-780, DOI:10.1038/nm.1987 (2009).
44. Chang, Z., Gao, Y., Chen, P., Gao, W., Zhao, W., Wu, D., . . . Xi, H. THBS2 promotes gastric cancer progression and stemness via the Notch signaling pathway. *Am J Cancer Res.* **14**, 3433-3450, DOI:10.62347/uxwk4038 (2024).
45. Adams, J. C. & Lawler, J. The thrombospondins. *Cold Spring Harb Perspect Biol.* **3**, a009712, DOI:10.1101/cshperspect.a009712 (2011).
46. Milosevic, A., Liebmann, T., Knudsen, M., Schintu, N., Svenningsson, P., & Greengard, P. Cell- and region-specific expression of depression-related protein p11 (S100a10) in the brain. *J Comp Neurol.* **525**, 955-975, DOI:10.1002/cne.24113 (2017).
47. Okura, G. C., Bharadwaj, A. G. & Waisman, D. M. Recent Advances in Molecular and Cellular Functions of S100A10. *Biomolecules.* **13**, DOI:10.3390/biom13101450 (2023).
48. Satooka, H., Nagakubo, D., Sato, T. & Hirata, T. The ERM Protein Moesin Regulates CD8(+) Regulatory T Cell Homeostasis and Self-Tolerance. . *J Immunol.* **199**, 3418-3426, DOI:10.4049/jimmunol.1700074 (2017).
49. Wang, Y., Yin, Q., Yang, D., Jin, H., Yao, Y., Song, J., . . . Zhao, H. LCP1 knockdown in monocyte-derived macrophages: mitigating ischemic brain injury and shaping immune cell signaling and metabolism. *Theranostics.* **14**, 159-175, DOI:10.7150/thno.88678 (2024).
50. Liu, R., Wang, J., Chen, Y., Collier, J. M., Capuk, O., Jin, S., . . . Begum, G. NOX activation in reactive astrocytes regulates astrocytic LCN2 expression and neurodegeneration. *Cell Death Dis.* **13**, 371, DOI:10.1038/s41419-022-04831-8 (2022).
51. Wang, G., Weng, Y. C., Han, X., Whaley, J. D., McCrae, K. R., & Chou, W. H. Lipocalin-2 released in response to cerebral ischaemia mediates reperfusion injury in mice.*J Cell Mol Med.* **19**, 1637-1645, DOI:10.1111/jcmm.12538 (2015).
52. Cha, J. H., Wee, H. J., Seo, J. H., Ahn, B. J., Park, J. H., Yang, J. M., . . . Kim, K. W. AKAP12 mediates barrier functions of fibrotic scars during CNS repair. *PLoS One.* **9**, e94695, DOI:10.1371/journal.pone.0094695 (2014).
53. Chen, W., Liu, K., Wang, Z., Zhang, H., Tan, M., Liu, Y., . . . Cheng, S. Migrasome-related ITGA5 for predicting prognosis, immune infiltration and drug sensitivity of hepatocellular carcinoma. *Apoptosis.*

DOI:10.1007/s10495-025-02103-2 (2025).

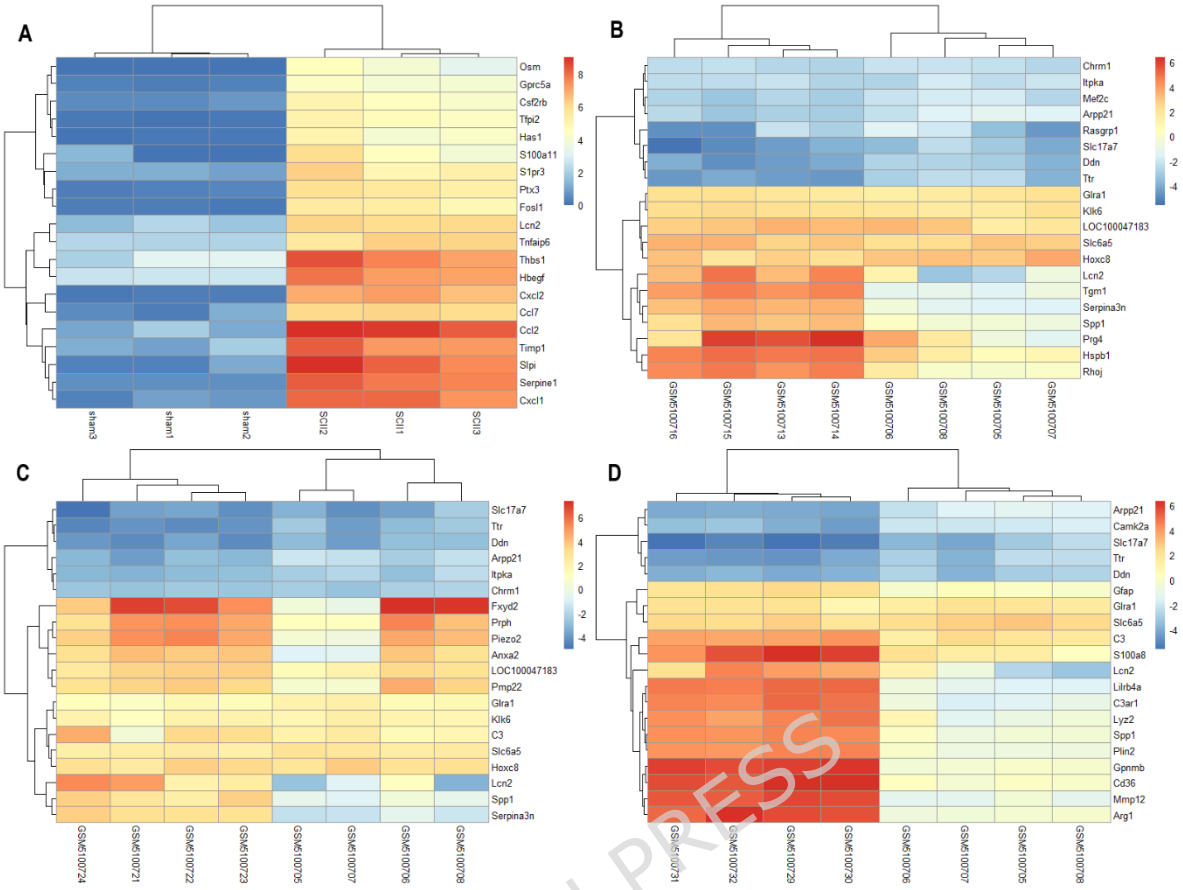

Figure 1. Heatmaps of GSE138966 and GSE167274 to observe the trends of the expression of differentially expressed genes (DEGs). The red area indicates high gene expression, while the blue area indicates low expression.

A. Heatmap for top 20 DEGs between control and SCII groups at 48 hours after rat SCII in GSE138966. B. Heatmap for top 20 DEGs between control and SCII groups at 1-day after C57BL/6J mice SCII in GSE167274

C. Heatmap for top 20 DEGs between control and SCII groups at 3-day after C57BL/6J mice SCII in GSE167274

D. Heatmap for top 20 DEGs between control and SCII groups at 7-day after C57BL/6J mice SCII in GSE167274

DEGs are sorted in descending order by the absolute value of logFC, and the top 20 DEGs are selected for heatmap visualization.

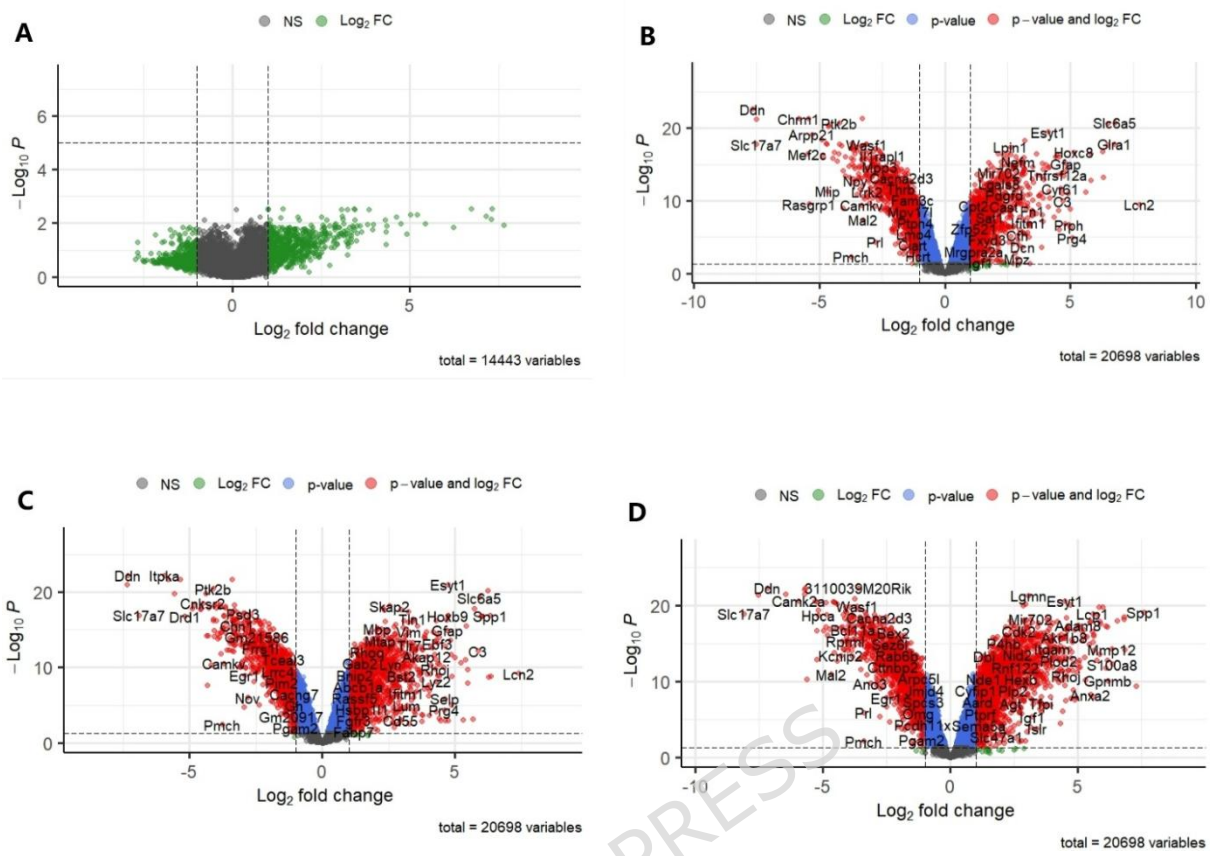

Figure 2. Volcano plots revealed the differentially expressed genes (DEGs) of the spinal cord ischemia injury (SCII) samples compared to the controls in GSE138966 and GSE167274

A. Volcano plot for DEGs between control and SCII groups at 48 hours after rat SCII in GSE138966 (|logFC| > 1& P.adj < 0.05)

B. Volcano plot for DEGs between control and SCII groups at 1-day after C57BL/6J mice SCII in GSE167274 (|logFC| > 1& P.adj < 0.05)

C. Volcano plot for DEGs between control and SCII groups at 3-day after C57BL/6J mice SCII in GSE167274 (|logFC| > 1& P.adj < 0.05)

D. Volcano plot for DEGs between control and SCII groups at 7-day after C57BL/6J mice SCII in GSE167274 (|logFC| > 1& P.adj < 0.05)

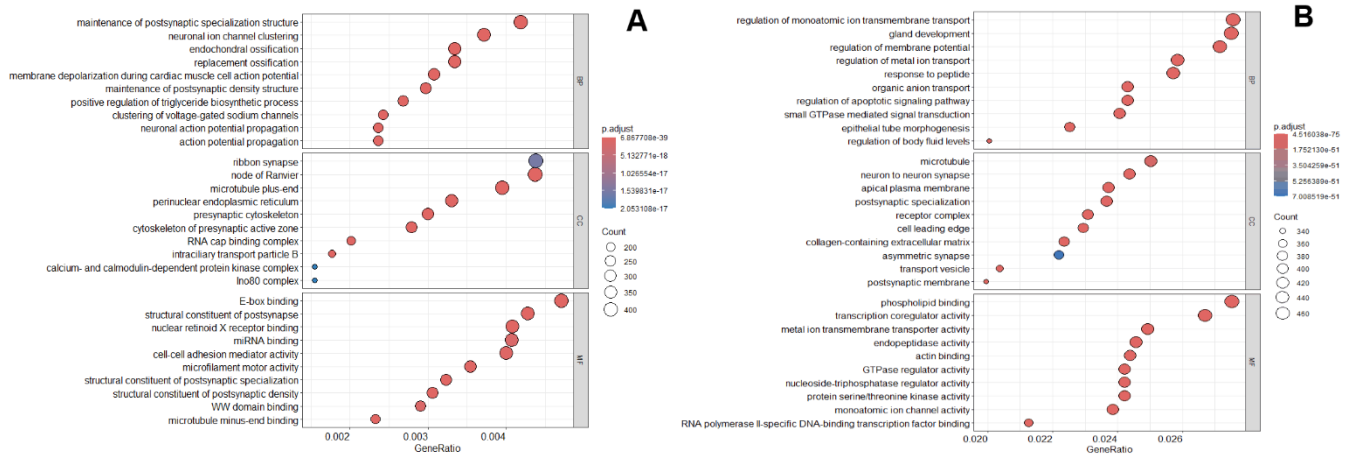

Figure 3. GO function enrichment in GSE138966 and GSE167274

A. The dotplot representing TOP 10 biological processes (BP), cellular components (CC) and molecular functions (MF) of GO analysis of differentially expressed genes (DEGs) in GSE138966; .

B. The dotplot representing TOP 10 BP, CC and MF of GO analysis of DEGs in GSE167274, the results of 1-day, 3-day and 7-day in C57BL/6J mice spinal cord ischemia are the same.

Color indicates p.adj; node size indicates the number of genes enriched in GO terms.

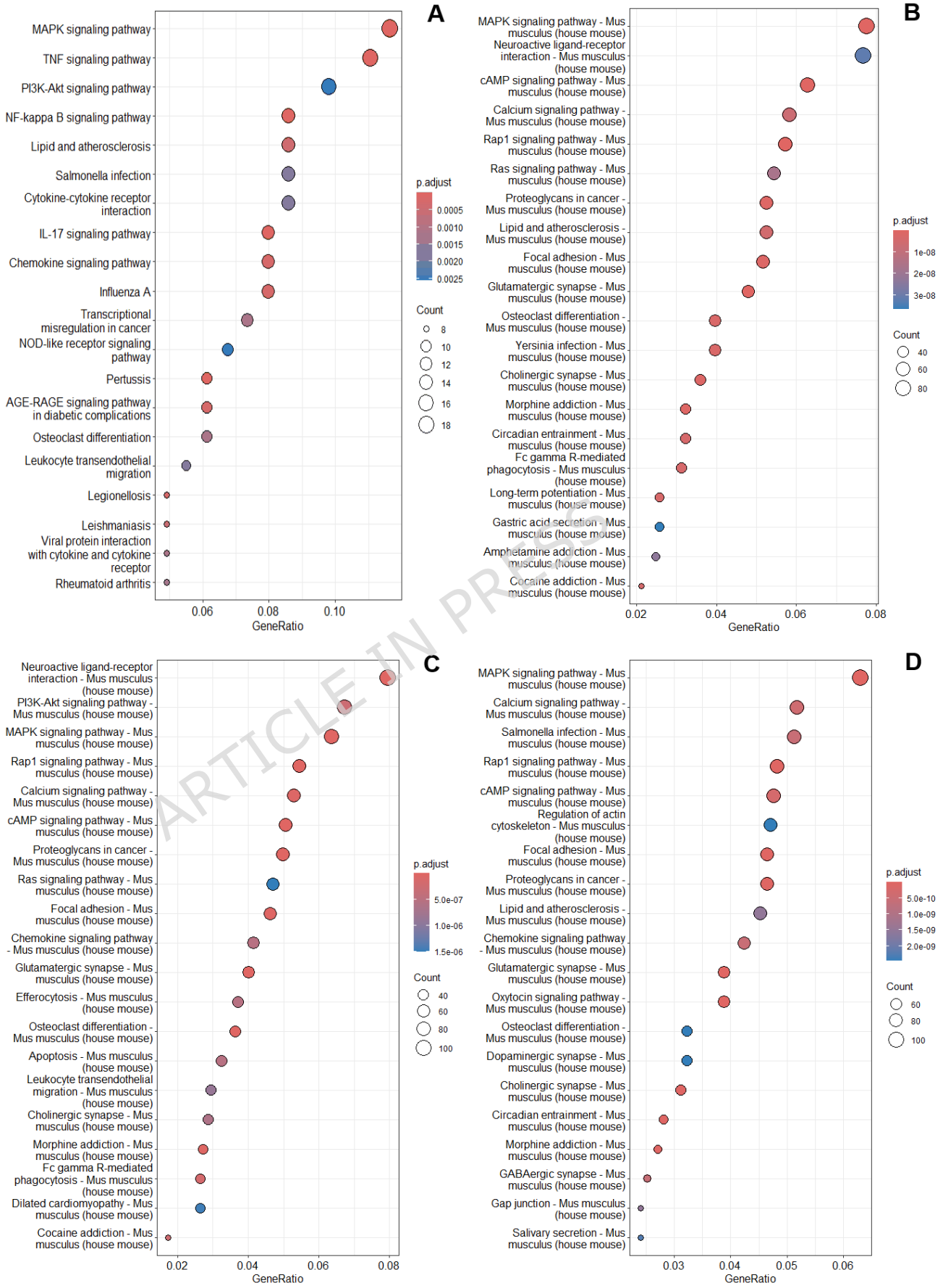

Figure 4. KEGG function enrichment in GSE138966 and GSE167274

A. The dotplot for TOP 20 KEGG pathway analysis of DEGs at 48 hour after rat spinal cord ischemia injury (SCII) in GSE138966;

B. The dotplot for TOP 20 KEGG pathway analysis of DEGs at 1-day after C57BL/6J mice SCII in GSE167274;

C. The dotplot for TOP 20 KEGG pathway analysis of DEGs at 3-day after C57BL/6J mice SCII in GSE167274;

D. The dotplot for TOP 20 KEGG pathway analysis of DEGs at 7-day after C57BL/6J mice SCII in GSE167274;

Vertical coordinate shows KEGG terms; node size indicates the number of genes enriched in the pathway; node color indicates p.adj.

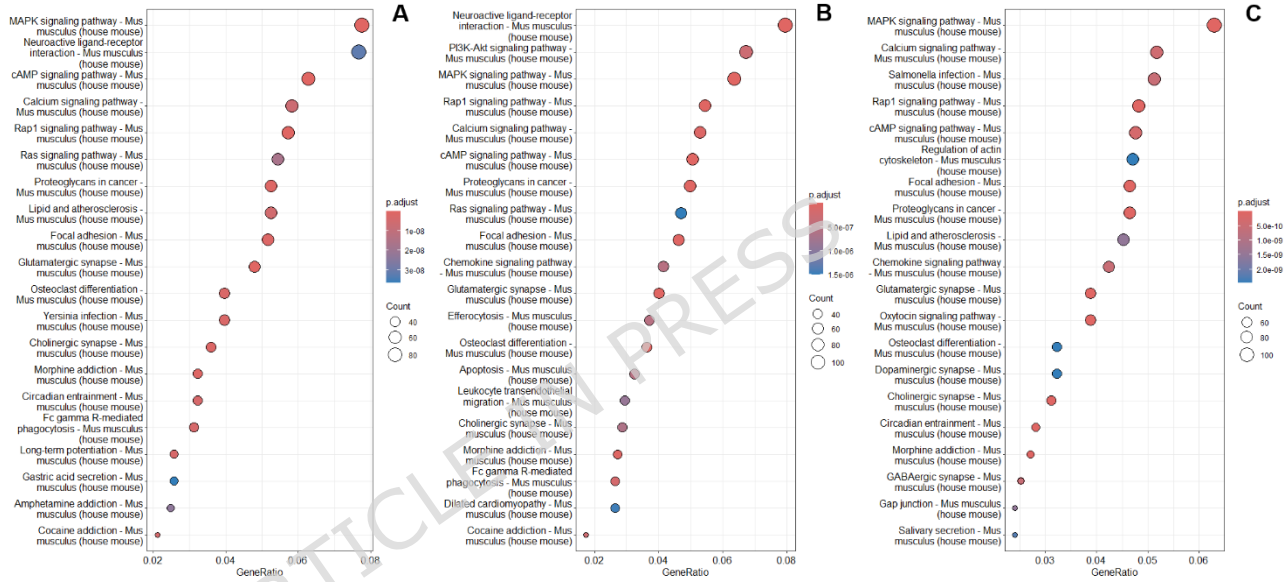

Figure 5. dotplot for KEGG at different time points after spinal cord ischemia injury (SCII) in GSE167274

A. The dotplot for TOP 20 KEGG pathway re-analysis of DEGs at 1-day after C57BL/6J mice SCII in GSE167274.

B. The dotplot for TOP 20 KEGG pathway re-analysis of DEGs at 3-day after C57BL/6J mice SCII in GSE167274.

C. The dotplot for TOP 20 KEGG pathway re-analysis of DEGs at 7-day after C57BL/6J mice SCII in GSE167274.

Vertical coordinate shows the GO terms; node size indicates the number of genes enriched in the pathway; node color indicates p.adj.

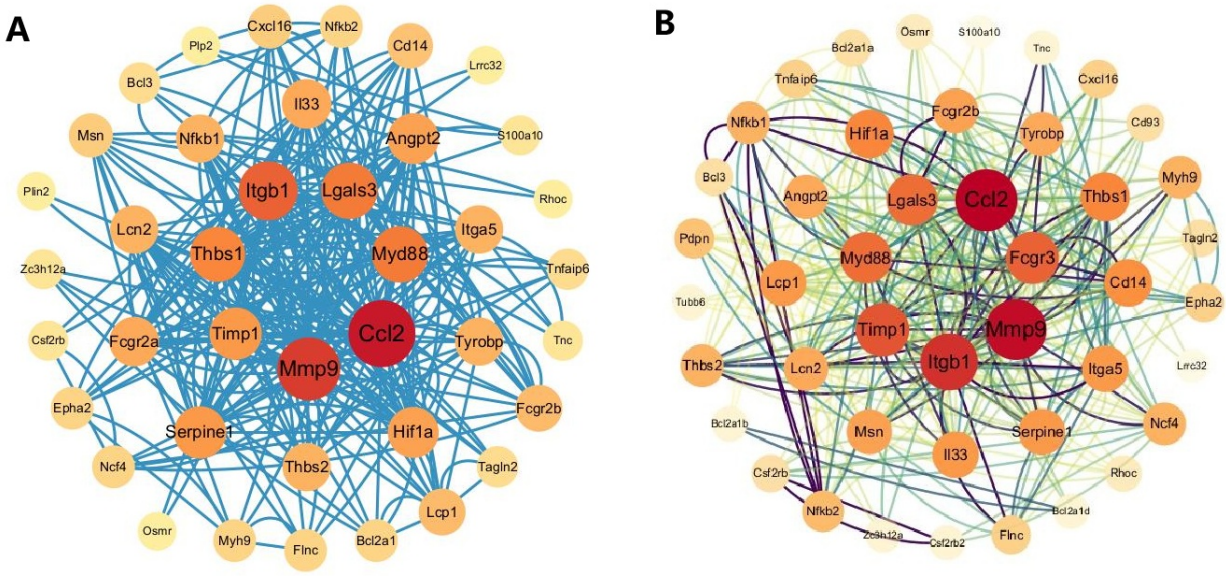

Figure 6. PPI network.

A total of 64 hub DEGs after homology analysis (|log2FC| > 1, P.adj < 0.05) were constructed respectively via STRING and visualized in Cytoscape in GSE138966 and GSE167274 (Red nodes with thick dark blue edges indicates a high-degree node, while yellow nodes with thin light blue edges denotes low-degree nodes).

A. Organism selection: Rattus norvegicus; After analysis using String website, 44 nodes and 364 edges are obtained.

B. Organism selection: Mus musculus; After analysis using String website, 40 nodes and 274 edges are obtained.

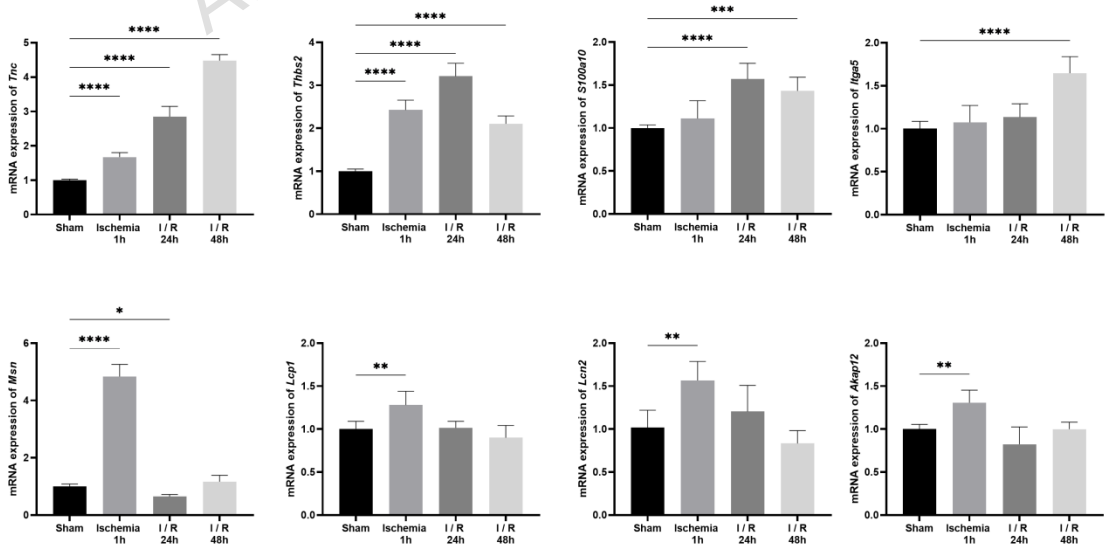

Figure 7. The mRNA expression of Hub Genes at different time points following spinal cord ischemia

Compared with sham group, the expression levels of *TNC*, *THBS2*, *S100A10* at 1h, 24h and 48h after ischemia were increased. Meanwhile, the expression of *MSN*, *LCP1*, *LCN*2 and *AKAP12* were increased at 1h after ischemia, and the expression of *ITGA5* was increased at 48h after ischemia. I/R, spinal cord ischemia-reperfusion. *P < 0.05 vs Sham group.

Student's t-tests were used, and all statistical tests were two-sided.